Open Research Online

The Open University's repository of research publications
and other research outputs

Isotopically Heavy Micrometeorites—Fragments of CY Chondrite or a New Hydrous Parent Body?

Journal Item

oro.open.ac.uk

Isotopically Heavy Micrometeorites—Fragments of CY Chondrite or a New Hydrous Parent Body?

M. D. Suttle[1,2,3] [ID]**, L. Folco[1,4]** [ID]**, Z. Dionnet[5,6], M. Van Ginneken[7]** [ID]**, T. Di Rocco[8], A. Pack[8]** [ID]**, M. Scheel[9], and A. Rotundi[6]**

[1]Dipartimento di Scienze della Terra, Università di Pisa, Pisa, Italy, [2]Planetary Materials Group, Natural History Museum, London, UK, [3]School of Physical Sciences, The Open University, Milton Keynes, UK, [4]CISUP, Centro per l'Integrazione della Strumentazione dell'Università di Pisa, Pisa, Italy, [5]Institut d'Astrophysique Spatiale, Université Paris-Saclay, Gif-sur-Yvette, France, [6]DIST-Università di Napoli "Parthenope", Centro Direzionale Isola C4, Naples, Italy, [7]Centre for Astrophysics and Planetary Science, School of Physical Sciences, University of Kent, Canterbury, UK, [8]Geowissenschaftliches Zentrum, Universität Göttingen, Göttingen, Germany, [9]Synchrotron SOLEIL, Saint-Aubin, France

Abstract Cosmic dust grains sample a diverse range of solar system small bodies. This includes asteroids that are not otherwise represented in our meteorite collections. In this work we obtained 3D images of micrometeorite interiors using tomography before collecting destructive high-precision oxygen isotope measurements. These data allow us to link textures in unmelted micrometeorites to known chondrite groups. In addition to identifying particles from ordinary chondrites, CR and CM chondrites we report two micrometeorites derived from an anomalous ^{16}O-poor source (δ^{17}O: +16.4‰, δ^{18}O: +28.4‰, and Δ^{17}O: +1.4‰). Their compositions overlap with a previously reported micrometeorite (TAM50-25) from Suttle et al. (2020), https://doi.org/10.1016/j.epsl.2020.116444 (EPSL: 546:116444). These particles represent hydrated carbonaceous chondrite material derived either from a new group or from the CY chondrites (thereby extending the isotopic range of this group). In either scenario they demonstrate close petrographic and isotopic connections to the CO-CM chondrite clan. Furthermore, their position in O-isotope space makes them the most likely candidate for the parent body of the anomalous "group 4" cosmic spherules previously reported by Suavet et al. (2010), https://doi.org/10.1016/j.epsl.2010.02.046 (EPSL: 293:313-320) and several subsequent isotopic studies. We conclude that the "group 4" cosmic spherules originate from hydrated C-type asteroid parents.

Plain Language Summary One of the principal aims of planetary science is to understand the origin and formation of our solar system. Studying primitive extraterrestrial material found at the Earth's surface allows us to explore the chemical composition of early formed solids which acted as the "building blocks" for planet formation. Most research analyses large (centimeter and bigger) meteorites. Here, we investigated the smaller size fractions (cosmic dust) using a combination of tomography to image particle interiors and destructive mass spectrometry to measure their oxygen isotope compositions. We identify two anomalous particles containing abundant heavy oxygen. These grains are part of the carbonaceous chondrite super group but appear to sample a new and otherwise unstudied group. This discovery is significant because it broadens our awareness of the geological diversity of the asteroid belt and compositional variation that existed among planetesimals in the early solar system.

1. Introduction

Asteroids and comets release dust into interplanetary space through collisions and sublimation. These grains then spiral into the inner solar system due to P-R drag—a non-gravitational force that decays the orbits of small objects (Burns et al., 1979). Some of the cosmic dust that reaches 1 AU is captured by Earth's gravitational field. Current estimates suggest ~40,000 tons of dust fall to Earth each year (Love & Brownlee, 1993). Most infalling grains are vaporized during atmospheric entry (>90%, Taylor et al., 1998) although some particles survive to the surface.

The study of cosmic dust provides planetary scientists with an opportunity to explore the vast array dust-producing bodies in our solar system. Because unmelted and partially melted (termed scoriaceous) micrometeorites retain much of their pre-atmospheric mineralogy and textures they allow us to study the geological properties of their parent bodies. This is in contrast to analyzing melted micrometeorites (termed cosmic spherules) which retain only the geochemical and isotope signatures of the parent body, partially overprinted by atmospheric entry processes (Baecker et al., 2018; Cordier et al., 2011; Goderis et al., 2020; Rudraswami et al., 2022; Suavet et al., 2010).

Numerous studies have demonstrated that different types of parent body are more abundant at different size fractions. For example, fine-grained, carbon-rich micrometeorites, assumed to originate from comets (Noguchi et al., 2015) are found primarily among the smallest size fractions (<100 μm), while the proportion of ordinary chondrite (OC) material increases significantly with increasing particle diameter (Cordier & Folco, 2014). Despite these variations, at every size fraction, fine-grained micrometeorites which originate from hydrated carbonaceous chondrite parent bodies are the most abundant type of micrometeorite (Taylor et al., 2012). They are probably sampling a wide range of dust-producing C-type asteroids. Many of these grains have geochemical, textural and mineralogical affinities to the CM, CR and CI chondrite groups (Cordier & Folco, 2014; Kurat et al., 1994; Suttle et al., 2020; Taylor et al., 2012; Van Ginneken et al., 2012). However, distinct differences suggest that the micrometeorite flux also contains a wealth of otherwise unsampled chondritic asteroids, which are not represented among our meteorite collections (Battandier et al., 2018; Dobrică et al., 2019; Engrand & Maurette, 1998). Studying cosmic dust therefore means we are able to greatly expand the number of known parent bodies and thus to more accurately investigate the geological diversity of the asteroid belt.

In this study were focus on a population ($N = 11$) of large micrometeorites (420–820 μm), most of which are either unmelted or scoriaceous particles. We use μ-CT to non-destructively image their interiors, facilitating classification, textural analysis and allowing mineralogy to be inferred. Particles were then analyzed destructively by laser fluorination O-isotope mass spectrometry. We use the resulting high-precision O-isotope compositions, coupled with their petrography to assign a probable parent body to each micrometeorite. In most instances we are able to confidently link particles to a known chondrite group. However, two particles have distinct isotopically heavy ^{16}O-poor compositions. They may record the pre-atmospheric O-isotope composition of the previously reported anomalous "group 4" class of cosmic spherules originally described by Suavet et al. (2010). Their composition is consistent with a water-rich parent asteroid (Suttle et al., 2020). We explore the significance of this finding and discuss the potential relationship this new material to established carbonaceous chondrites.

2. Materials and Methods

Micrometeorites analyzed in this study were recovered from the summit of Miller Butte in the Transantarctic Mountains (TAM) by members of the 2009 Italian PNRA (Programma Nazionale di Ricerche in Antartide) expedition. All particles investigated here were extracted from a single sediment trap (termed TAM45). Details of the geological site, the mechanism of cosmic dust accumulation and the approximate age of the trap (between 800,000 years and 2 million years) can be found in Rochette et al. (2008) and Suttle and Folco (2020).

Whole micrometeorites were imaged under scanning electron microscope (SEM) without coating at the Centro per l'Integrazione della Strumentazione dell'Università di Pisa using a FEI Quanta 450 field emission gun SEM, operating at 20 keV and low-vacuum mode (90 Pa). This allowed us to obtain morphological and petrographic data on their external surfaces for a broad classification into unmelted and partly melted (termed scoriaceous) micrometeorite groups, according to Genge et al. (2008) and Folco and Cordier (2015).

Micro-CT scans were collected at the SOLEIL synchrotron (France) on the ANATOMIX beamline. This provided textural and compositional data on their interiors, following (Dionnet et al., 2020). We used a monochromatic beam (16.87 keV) and achieved a voxel size of 0.325 μm. We measured 2D projections of the linear attenuation coefficient (LAC) at regular rotation intervals to generate a model of LAC variation in 3D. Postprocessing employed the academic software PyHST2 (Mirone et al., 2014). We performed a 3D evaluation of each particle's porosity, following the technique outlined in Dionnet et al. (2020). We note that when using hard x-rays to image micrometeorite interiors the resulting LAC is insensitive to low-Z materials (low atomic number), notably organic matter. This means that some of the dark voxels within our samples that were classified as empty voids may instead contain limited organic matter, for example, as nanometric globules (Matrajt et al., 2012). Although the omission of organic matter is unlikely to have a substantial effect of the calculated porosity values it should be remembered that porosity estimates quoted here are upper limits.

Triple oxygen isotope measurements were carried out at the Geowissenschaftliches Zentrum, University of Göttingen, by infrared (IR) laser fluorination method (Sharp, 1990) in combination with a Thermo MAT253 IRMS. Prior to analysis, the samples were leached in ethanolamine thioglycolate to remove traces of terrestrial alteration (Greenwood et al., 2012). Afterward, aliquots of approximately 150 μg were placed, together with similar amounts of San Carlos olivine and UWG garnet (Table 1) in a 14 pit sample holder. The sample holder was

Table 1

Triple O-Isotope Measurements Performed on Our Reference Mineral Standards (San Carlos Olivine and UWG)

ID	Sample	Sample mass (μg)	$\delta^{17}O$	$\delta^{18}O$	$\Delta'^{17}O$
9720	San Carlos 0820	199	2.563	4.970	−0.058
9766		180	2.531	4.922	−0.065
9764		170	2.831	5.453	−0.045
9830		150	2.623	5.067	−0.048
9714		149	2.860	5.510	−0.046
9765		135	2.748	5.314	−0.054
9778		96	2.732	5.275	−0.049
9709	UWG200	177	3.154	6.149	−0.088
9826		169	2.929	5.676	−0.064
9834		161	2.915	5.641	−0.059
9828		152	2.929	5.683	−0.067
9767		102	2.854	5.519	−0.056

Note. They are of similar masses to the micrometeorites studied in this work (given in Table 2). Analyses are ordered by sample mass (largest to smallest).

then loaded into a reaction chamber and evacuated overnight. Each sample was fluorinated in the presence of 100 mbar of BrF_5. The extraction and purification of O_2 was performed by employing the same line and similar protocol as in Pack et al. (2016). The purified O_2 was then transferred via He gas stream (10 mL min⁻¹) into a 5 Å molecular sieve trap located in front of the mass spectrometer. After evacuation of He from this trap, O_2 was captured at −195°C into the internal microvolume inlet of the MAT253, filled with 5 Å molecular sieve and then expanded into the mass spectrometer source at 50°C. $^{18}O/^{16}O$ and $^{17}O/^{16}O$ values are expressed in conventional delta notation ($\delta^{17}O$ and $\delta^{18}O$) relative to VSMOW. For mass dependent processes, variations in $\delta^{17}O$ are about half of variations in $\delta^{18}O$. Deviations from such a mass dependent fractionation line are expressed in form of the $\Delta^{17}O$ notation (Equation 1) with:

$$\Delta^{17}O = \delta^{17}O - 0.52 \cdot \delta^{18}O \qquad (1)$$

Measured isotopic values are anchored to VSMOW using the composition of San Carlos olivine and UWG2 garnet (Pack, 2021; Pack et al., 2016; Sharp et al., 2016; Wostbrock et al., 2020). Data reduction was performed using either offset correction or intensity correction as required. All raw data and intensity values can be found in the Data Set S1. On the basis of replicate analyses of San Carlos olivine and UWG2 garnet, the analytical uncertainties in $\delta^{18}O$, $\delta^{17}O$, and $\Delta^{17}O$ are ±0.4‰, ±0.2‰, and ±0.024‰ (2σ), respectively.

3. Results

We analyzed 11 micrometeorites (Figure 1), with diameters between 420 and 820 μm and masses between 0.14 and 0.71 mg. All particles are whole micrometeorites with subangular to subrounded shapes. Their external surfaces exhibit well-developed magnetite rims and in some particles are encrusted by terrestrial weathering products (Van Ginneken et al., 2016). Micro-CT scans (Figure 2) revealed their internal textures, facilitating classification (Genge et al., 2008). Our population includes six fine-grained micrometeorites, two coarse-grained micrometeorites, one composite particle as well as two cosmic spherules of the porphyritic subgroup (PO). Calculated porosities vary between 7.9 and 44.1 vol%. In general, porosities below 20 vol% correspond to unmelted particles, while higher porosities are typical of scoriaceous micrometeorites.

Bulk O-isotope compositions (Table 2, Figure 3) vary between $\delta^{17}O$: −0.7‰ and +19.2‰, $\delta^{18}O$: +0.6‰ and +34.7‰, and $\Delta^{17}O$: −4.8‰ and +1.4‰. Four micrometeorites plot above the terrestrial fractionation line (TFL), seven plot below.

4. Discussion

4.1. Alteration During Atmospheric Entry

The parent bodies of micrometeorites can be inferred through analysis of their composition and textures (e.g., Cordier et al., 2018). However, interpretation is complicated by the effects of atmospheric entry heating which progressively overprint the pre-atmospheric properties of micrometeorites as a function of increasing peak temperatures and heating duration (Toppani et al., 2001). A robust understanding of the atmospheric entry process is essential if a micrometeorite's origins are to be accurately interpreted.

During the early stages of flash heating, at sub-solidus temperatures, heat-sensitive phases (e.g., phyllosilicates, carbonates, sulfides, and organic matter) rapidly decompose, releasing volatile gases (Greshake et al., 1998; Suttle et al., 2019; Taylor et al., 2011). Temperature gradients may be established where the thermal decomposition of phyllosilicate acts as an efficient heat sink, allowing the core temperatures in micrometeorites to remain relatively low (Genge et al., 2017). Dehydration reactions result in volume contractions that may cause the particle to fragment (Suttle, Genge, & Russell, 2017). With continued heating dehydrated phyllosilicate recrystallize to from anhydrous olivine and pyroxene (Greshake et al., 1998; Suttle, Genge, Folco, et al., 2017). As peak

Figure 1. (A–K) External BSE images for each of the 11 micrometeorites analyzed in this study. (L) Also included is the anomalous ^{16}O-poor micrometeorite published in Suttle et al. (2020) TAM50-25. Parent body interpretations are given for each particle (shown in yellow).

temperatures exceed the solidus of chondritic materials (approximately $T > 1000°C$ (Toppani et al., 2001)) a melt layer forms of the particle exterior, referred to as an igneous rim (Genge, 2006). Complete melting occurs at $T > 1400°C$ (Toppani et al., 2001), forming cosmic spherules. In general, large coarse-grained anhydrous minerals are preferentially preserved over fine-grained matrix. However, often hydrated phyllosilicate textures may be preserved because phyllosilicates readily dehydrate and recrystallize, forming nanophase olivine before the onset of melting (Suttle, Genge, Folco, et al., 2017).

As explained in Suavet et al. (2010) the O-isotope composition of micrometeorites is affected by two competing processes: evaporation and mixing. Evaporation results in a preferential loss of isotopically light oxygen and is, therefore, a mass-dependent fractionation process. This causes a particle's bulk composition to migrate toward heavier ^{18}O-rich compositions (moving on a ~0.52 slope in $\delta^{17}O/\delta^{18}O$ isotope space, parallel to the TFL). Meanwhile mixing with atmospheric oxygen draws a particle's composition toward terrestrial values. Because entry
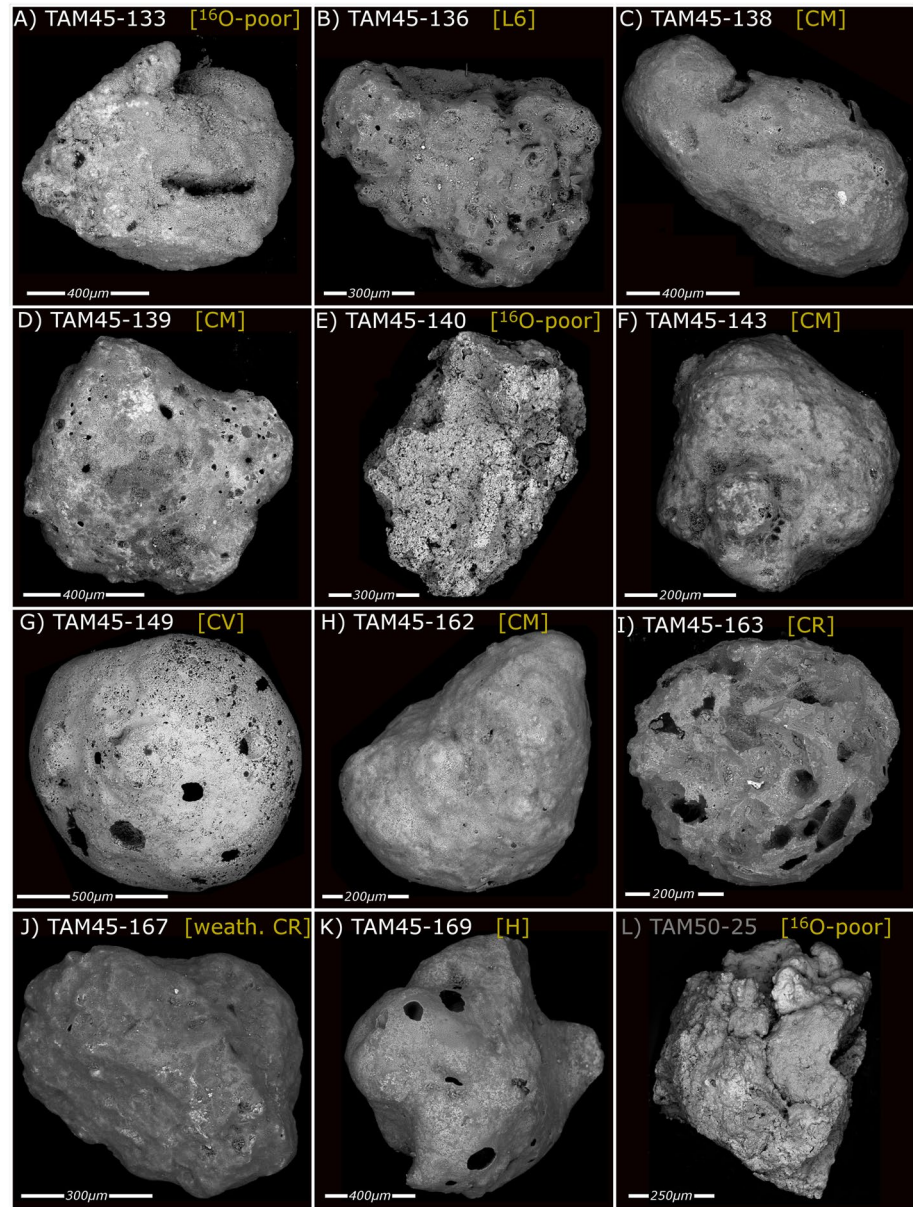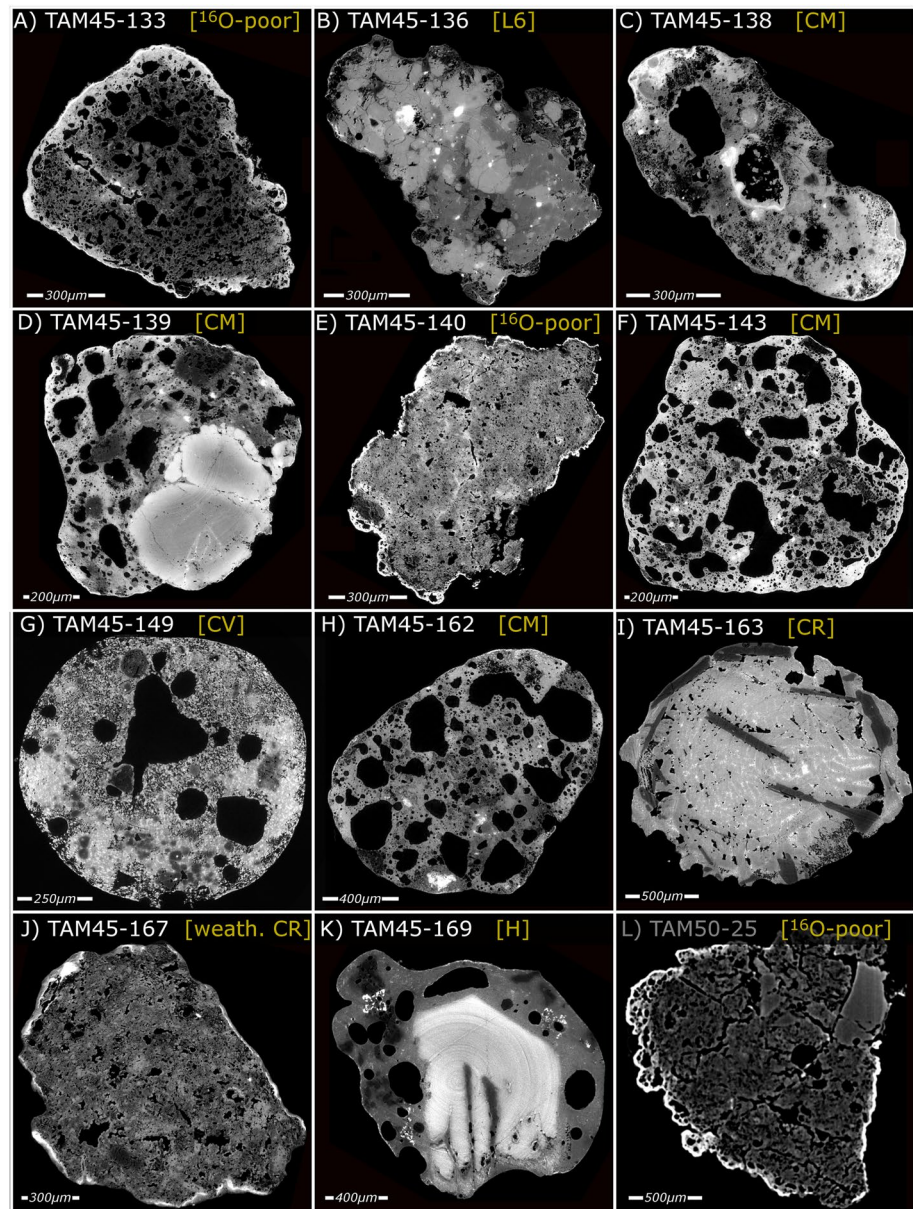
Figure 2. (A–K) Example µCT slices for each of the 11 micrometeorites analyzed in this study. (L) Also included is the anomalous ^{16}O-poor micrometeorite published in Suttle et al. (2020) TAM50-25. Parent body interpretations are also given for each particle (shown in yellow). Note some images are affected by ring artifacts centered on the rotational axis of the particle arising due to shifts in the output efficiency of individual detectors. These rings should be ignored as they are not a petrographic feature of the samples (Ketcham & Carlson, 2001).

heating occurs at high altitudes, equilibration is assumed to occur with stratospheric oxygen whose composition is approximately δ^{17}O: +12.1‰, δ^{18}O: +23.9‰, and Δ^{17}O: −0.32‰ (Pack, 2021; Pack et al., 2017; Thiemens et al., 1995). The relative importance of evaporation and mixing on a micrometeorite's final O-isotope composition are dependent on the entry parameters (i.e., entry speed, entry angle, and therefore peak temperature and heating duration). However, recent work suggests that evaporative mass-dependent fractionation is more important that mixing (Rudrasawmi et al., 2020).

Table 2
The 11 Micrometeorites Investigated in This Study, Showing Their Sizes, Masses, μCT Data, and Triple O-Isotope Bulk Compositions

ID	Sample	Avg. size (μm)	Mass (mg)	Porosity (vol%)	Type	Entry heating	Distinctive features	$\delta^{17}O$	$\pm 2\sigma$	$\delta^{18}O$	$\pm 2\sigma$	$\Delta^{17}O$	$\pm 2\sigma$	Class	Subclass	Notes
						Data from μCT				O-isotope data, relative to VSMOW (‰)				Interpretation – Parent body		
1	TAM45-133	640	0.35	33.8	FgMM	Scoriaceous	Highly porous, anhydrous silicates rare.	19.215	0.2	34.739	0.4	0.873	0.024	Carb. Chondr.	^{16}O-poor	Close to the anom. Group 4 cosmic spherule population
2	TAM45-136	700	0.38	7.9	CgMM	Unmelted	Coarse, interlocking crystalline texture	4.550	0.2	7.042	0.4	0.831	0.024	Ordin. Chondr.	L	Metamorphosed, likely an L6
3	TAM45-138	750	0.71	20	FgMM	Scoriaceous	Fine-grained matrix and elongated shape, Fe-rich phases at ends, large vesicle in center	3.184	0.2	12.625	0.4	−3.482	0.024	Carb. Chondr.	CM	High spin rate during atmospheric entry
4	TAM45-139	730	0.56	18.2	Comp.	Scoriaceous	Scoriaceous fine-grained matrix with large bright grain (chromite) and chondrules	5.630	0.2	14.559	0.4	−2.057	0.024	Carb. Chondr.	CM	Large chromites in a CC lithology are rare
5	TAM45-140	640	0.39	14.8	FgMM	Unmelted	Fine-grained compact texture, few anhydrous silicates, abundant Fe-rich phases (sulfides)	16.382	0.2	28.384	0.4	1.395	0.024	Carb. Chondr.	^{16}O-poor	Contains small chondrule pseudomorphs
6	TAM45-143	790	0.29	41.1	FgMM	Scoriaceous	Highly porous, abundant Fe-rich phases (sulfides)	9.788	0.2	23.232	0.4	−2.479	0.024	Carb. Chondr.	CM or CY	One large chondrule pseudomorph visible
7	TAM45-149	820	0.70	31.8	CS-PO	Mostly melted	Fine-grained crystalline groundmass w/ porphyritic chondrules	−0.206	0.2	8.709	0.4	−4.804	0.024	Carb. Chondr.	CV	fine-grained crystalline matrix consistent with a CV precursor
8	TAM45-162	520	0.33	44.1	FgMM	Scoriaceous	Highly porous, abundant Fe-rich phases (sulfides)	6.656	0.2	17.485	0.4	−2.576	0.024	Carb. Chondr.	CM or CY	A "typical" Sc-FgMM texture
9	TAM45-163	490	0.15	13.3	CS-PO	Melted	Abundant Fe-rich interstitial phase and long acicular anhydr. silicates.	1.201	0.2	5.118	0.4	−1.502	0.024	Carb. Chondr.	CR	Chondrule material from the CR lithology
10	TAM45-167	520	0.14	12.6	FgMM	Unmelted	Fine-grained compact texture, few anhydrous silicates	−0.666	0.2	0.626	0.4	−0.997	0.024	Carb. Chondr.	CR	Affected by weathering producing mixing toward SLAP
11	TAM45-169	420	0.16	15.8	CgMM	Scoriaceous	Large hexagonal bright grain (chromite) in glassy groundmass	4.995	0.2	9.051	0.4	0.216	0.024	Ordin. Chondr.	H	Isotope composition must be dominated by chromite grain

Note. On the basis of these data their inferred parent bodies are given alongside additional notes on any unusual features or further interpretations.
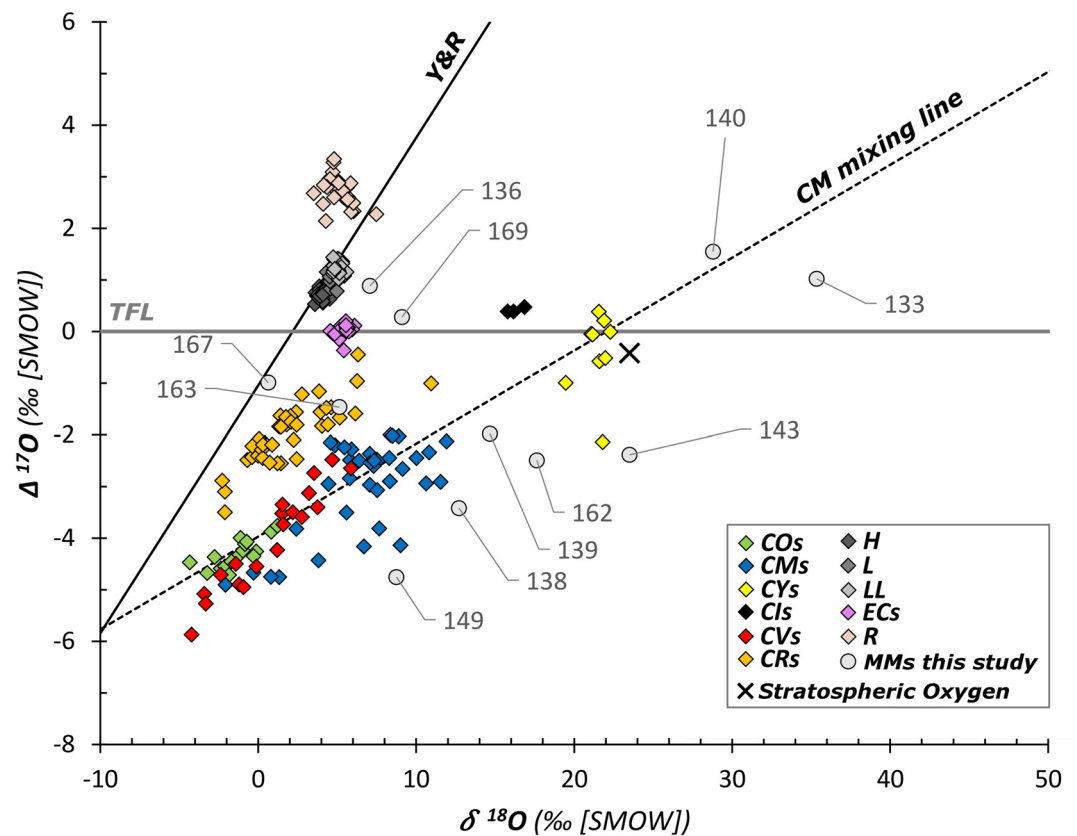
Figure 3. Bulk O-isotope compositions for the 11 micrometeorites analyzed in this study (gray circles), displayed on a $\delta^{18}O$ versus $\Delta^{17}O$ plot. Note, analytical uncertainties ($\delta^{18}O$: ± 0.4‰ and $\Delta^{17}O$: ± 0.024‰) are smaller than the symbols. Also shown for reference are data points for the established chondrite groups (colored diamonds) and the composition of terrestrial stratospheric oxygen (black cross symbol, Thiemens et al., 1995). The following isotopic reference lines are plotted: the TFL, the Y&R line and the CM mixing line (defined in Clayton and Mayeda (1999)). Chondrite data were taken from Clayton et al. (1984, 1991), Clayton and Mayeda (1996, 1999), Weisberg et al. (1996), Moriarty et al. (2009), Ivanova et al. (2010), Bischoff et al. (2011), Schrader et al. (2011, 2014), Lee et al. (2016, 2019), Bouvier, Gattacceca, Agee, et al. (2017), Bouvier, Gattacceca, Grossman, et al. (2017), King, Russell, et al. (2019), Gattacceca et al. (2019), and Kimura et al. (2020).

4.2. Micrometeorites Matched to Established Chondrite Groups

Eight of the 11 particles analyzed in this study can be confidently matched to known chondrite groups while a single particle appears to be a chondrule fragment from a carbonaceous chondrite parent body.

4.2.1. Non-Carbonaceous Chondrites

Particle TAM45-136 (Figures 1 and 2) shows a clear affinity to the OCs. It's O-isotope composition plots above the TFL and close to the OC field, slightly shifted to heavier values (due to mass-dependent fractionation during evaporative entry heating). TAM45-136 has a coarse-grained texture composed of interlocking crystals. Micro-CT data reveals rounded bright phases (most likely high atomic weight Fe-Ni metal), while the remaining phases are likely silicates. Based on their LAC grayscale values and texture they are interpreted as pyroxene (brightest gray and most abundant phase), olivine (middle gray) and interstitial plagioclase (darkest gray). The texture in TAM45-136 is therefore consistent with an equilibrated OC affected by high-grade metamorphism (namely, a high petrologic subtype).

Particle TAM45-169 also plots above the TFL and outside the OC field, again shifted to heavier (higher $\delta^{18}O$) values. However, the interpretation of TAM45-169's O-isotope composition is ambiguous because it's position could be explained either by an OC, an enstatite chondrite (EC) or a Howardite Eucrite Diogenite (HED) achondrite affected by mass-dependent fractionation during atmospheric entry. The particle's interior, as revealed by µCT is dominated by a single euhedral grain hundreds of microns in size with a high average atomic weight and

hexagonal outline. Because the grayscale value of this phase is brighter than the particle's magnetite rim, we infer the euhedral mineral is not composed of magnetite. Furthermore, Fe-sulfides (troilite, pyrrhotite, and pentlandite) are also ruled out because they suffer thermal decomposition at low temperatures (<800°C; King et al., 2015; Taylor et al., 2011) under open system conditions and would, therefore, not survive unmelted in a cosmic spherule. By contrast, chromite has both a higher average atomic weight than magnetite and is a refractory mineral, likely to survive atmospheric entry without significant melting (Heck et al., 2016; Rudraswami et al., 2019). Although, resorption textures are present on at least two sides of the grain, they are limited in extent, indicating only incipient melting at the grain margins. Thus, the bright phase in TAM45-169 is most likely chromite. If correct, the presence of chromite would favor an OC/HED over an EC parentage because chromite is relatively common as an accessory phase in the OCs (Wlotzka, 2005) and HEDs (Shearer et al., 2010), but absent from the ECs (e.g., Weisberg and Kimura, 2012). Determining between an OC or HED is not possible, however, we note that an OC parentage is more likely based upon previously reported micrometeorite statistics (Cordier and Folco, 2014).

4.2.2. CM Chondrites

Four particles (TAM45-138, TAM45-139, TAM45-143, and TAM45-162) are interpreted as originating from a CM or CM-like parent body. They have O-isotope compositions that plot close to the CM field, but mass fractionated to heavier values, having experienced, on average an increase of +5‰ to +10‰ in their $\delta^{18}O$ values during atmospheric entry. All four particles have scoriaceous textures and abundant rounded bright phases which are often seen abutting vesicles (likely Fe-sulfide melt beads, as described by Taylor et al. (2011)).

TAM45-138 has a strongly elongated "sausage shape" with an aspect ratio: 2.3:1 (Figures 1 and 2). Micro-CT reveals an interior in which bright Fe-rich phases are concentrated at the particle's extreme ends, while the particle center is dominated by a large empty vesicle. This shape combined with the distribution of phases strongly implies a high spin rate during atmospheric entry, producing a pronounced density-based separation of phases within the particle, as well as the observed elongation of the particle's shape perpendicular to the spin axis. A near-identical particle (TAM50-15) was reported by Dionnet et al. (2020). Despite the advanced state of partial melting in TAM45-138, residual chondrules can be resolved, they have subrounded shapes, which may be evidence of former aqueous alteration and silicate dissolution on the micrometeorite's parent body. This would be typical of CM chondrite materials.

TAM45-139 is a scoriaceous micrometeorite containing small (~140 μm) unmelted chondrules with a porphyritic texture. These are suspended in a glassy mesostasis, indicating that peak temperatures during atmospheric entry were high enough to melt and recrystallize the fine-grained matrix, whilst leaving the larger (Mg-rich) anhydrous silicates unaffected. This particle also contains a large (~300 × 500 μm) bright (high average atomic weight) inclusion (Figures 1 and 2), which is composed of two similar-sized grains as well as a series of smaller grains found along the inclusion's perimeter. All these grains have similar compositions (based on the μCT grayscale), although the two largest have clear evidence of compositional zonation and are affected by pervasive fractures, infilled with a brighter melt phase (forming veins). There are also numerous micro-scale voids within these grains. Because the grayscale value of this inclusion is similar to the particle's magnetite rim, we infer the inclusion is composed Fe, or similarly heavy elements. This inclusion is therefore likely a large anhedral chromite grain that suffered thermal fracture during atmospheric entry. The thermal fracture of anhydrous crystals in micrometeorites during entry is well documented and common among hydrated CM-like particles. This process is due to the large thermal gradients established across the igneous rim (Genge et al., 2017). If this scenario is correct, this would require that the original chromite was a single grain and during entry that subsequently suffered resorption, fracture into subgrains and chemical diffusion along fracture planes. The bright rim observed along the margin of the chromite grains would then reflect chemical exchange between the chromite and the surrounding micrometeorite's mesostasis.

TAM45-143 and TAM45-162 are petrographically very similar. They are dominated by a glassy silicate mesostasis with a highly vesicular texture. This network of vesicles also contains abundant unmelted anhydrous silicates and Fe-rich beads (either metal or sulfide). Few clues remain as to the particles' pre-atmospheric texture and mineralogy, preventing further deductions about their parent body provenance.

4.2.3. CR Chondrites

TAM45-167 (Figures 1 and 2j) is a fragment of fine-grained matrix, containing small rounded anhydrous silicates and some bright phases (either metal or Fe-sulfides). The O-isotope composition of this particle (Figure 3) plots close to CR field but shifted toward isotopically lighter values and close to the Young and Russell (1998) line (Y&R). Evidence for terrestrial weathering is clear from the encrustation shell on the particle exterior and growth of weathering phases within pore spaces inside the particle (Van Ginneken et al., 2016). As a result, we expect the O-isotope composition of TAM45-167 to be affected by partial equilibration with Antarctic water. This process shifts compositions toward lighter ^{16}O-rich compositions (Suttle et al., 2020) and therefore explains TAM45-167 otherwise lighter-than-expected composition.

4.2.4. A CM/CO/CV Source

One micrometeorite (TAM45-149; Figures 1 and 2) has ambiguous parentage. It is derived from a carbonaceous chondrite source but owing to the overlap of the CO, CV and CM chondrite fields in O-isotope space a single group cannot be resolved (Figure 3). This particle is a relic-bearing PO cosmic spherule with a high abundance of vesicles, preferentially concentrated in the particle's center, another common effect of high spin rates during atmospheric entry (Genge, 2017). Relict phenocrysts are clearly identified by their dark gray color in μCT images (Figure 2). They appear as rounded grains but also include a small microchondrule ($D < 40$ μm; Krot & Rubin (1996)) with a barred olivine texture. The groundmass is composed of small equant bright crystallites and light gray grains (interpreted as a mix of magnetite and Fe-rich olivine). A porous structure locally observed at the external margins and vesicles is probably due to Antarctic weathering which led to the dissolution of the silicate glass phase.

4.2.5. Loose Chondrule Material

TAM45-163 is a cosmic spherule with a microporphyritic texture. Relict grains appear as large dark subhedral acicular phenocrysts (interpreted as either Mg-rich silicates or plagioclase). They are concentrated at the particle's margin, indicating high spin rates during atmospheric entry (which can produce a centrifuge effect within the molten silicate micrometeorite (Dionnet et al., 2020; Genge, 2017; Genge et al., 2016)). Mesostasis phases include abundant light gray lath-shaped grains and an interstitial bright (Fe-rich) phase. The high degree of melting during atmospheric entry makes interpreting the parent body of TAM45-163 difficult. Its O-isotope composition plots well within the CR chondrite field, implying a direct link to the CR chondrites (Figure 3). However, given the large degree of entry heating the bulk O-isotope composition will have been strongly affected by mass fractionation (and potentially also mixing with atmospheric oxygen). As a result the pre-atmospheric composition would have been ^{16}O-enriched relative to what we measure (plotting to the left of its current position in Figure 3). Shifts in $\delta^{18}O$ by approximately $+10‰$ arising due to mass fractionation are typical for cosmic spherules (e.g., Rudraswami et al., 2020; Suavet et al., 2010). The corrected O-isotope composition of TAM45-163 would therefore remain below the TFL but positioned to the left of the Y&R line. This region of O-isotope space is typically occupied by primitive refractory inclusions found in chondrites (chondrules, CAIs, and AOAs (e.g., Yurimoto et al., 2008)). Based on the reconstructed O-isotope composition and the retention of dark acicular relict grains TAM45-163 is interpreted as chondrule material while it's precise parent body is unknown. Loose whole chondrules and chondrule fragments are frequently found among the micrometeorite flux, being relatively common at coarse size fractions (Genge et al., 2005, 2008; Van Ginneken et al., 2012). Although we have no additional information on the mineral species in TAM45-163 the dark relict grains could be plagioclase, in which case the micrometeorite would sample a former Al-rich chondrule.

4.3. Micrometeorites From a ^{16}O-Poor Source

Two micrometeorites (TAM45-140 and TAM45-133) have anomalous ^{16}O-poor compositions ($\delta^{17}O$: $+16.4‰$, $\delta^{18}O$: $+28.4‰$ and $\Delta^{17}O$: $+1.4‰$ and $\delta^{17}O$: $+19.2‰$, $\delta^{18}O$: $+34.7‰$, and $\Delta^{17}O$: $+0.9‰$, respectively). TAM45-133 (Figures 1a and 2a and 5a and 5b) is a scoriaceous particle with a well-developed vesicular texture, a thick (20–100 μm) igneous rim and a bright continuous magnetite rim. Clusters of bright rounded melt beads are preserved only near the particle's center (Figure 5a) and show an affinity for vesicles (they are therefore assumed to be volatile Fe-sulfide melt material (Taylor et al., 2011)). Anhydrous silicates are rare but appear as a single small cluster of grains interpreted as a chondrule with an approximate diameter of 170 μm (Figure 5b). This chondrule has a partially flattened shape ($200 \times 170 \times 140$ μm) and appears to have been significantly affected

by parent body aqueous alteration, as evidenced by the anhedral grain morphologies and etch textures within the chondrule core. TAM45-140 (Figures 1e and 2e and 5c and 5d) is less affected by atmospheric entry heating, as indicated by its thin igneous rim. Its internal texture is homogenous, compact and contains fewer voids, some of which have linear shapes. They are dehydration cracks formed when the phyllosilicate matrix dehydrated during atmospheric entry (Genge, 2006). TAM45-140 is composed entirely of mildly heated fine-grained matrix hosting small bright opaque grains (most likely magnetite and sulfides). There are no visible anhydrous silicates although a possible pseudomorphic chondrule is visible in the lower left corner of the image shown in Figure 2e—this measures $\sim 50 \times 100$ μm has a darker appearance (indicating a Mg-enriched composition). The possible pseudo-chondrule contains abundant aligned dehydration cracks, which may indicate the presence of a former petrofabric on the parent asteroid (Suttle, Genge, & Russell, 2017), similar to the low grade aligned phyllosilicates found in many CM chondrites (Lindgren et al., 2015). The very low abundance of anhydrous silicates (<5 vol%) in TAM45-133 and TAM45-140, combined with their phyllosilicate dominated matrices and the inferred presence of sulfides strongly suggest these particles are carbonaceous chondrites affected by advanced aqueous alteration.

The textures and isotopic composition of TAM45-140 and TAM45-133 are strikingly similar to another previously reported unmelted micrometeorite (TAM50-25, Suttle et al., 2020) and shown here in Figures 1l, 2l, 5e and 5f. All three particles likely originate from a single parent body source. Their position in O-isotope space is interesting for two reasons:

1. The three micrometeorites (TAM45-140, TAM45-133, and TAM50-25 [Figure 5]) plot in a region of O-isotope space far-removed from all previously reported chondritic meteorites (Figure 3). In addition, the unmelted TAM45-140 and TAM50-25 plot on the "*CM mixing line*" while the scoriaceous TAM45-133 is close to this line but mass-fractionated to heavier values (reflecting the mild effects of atmospheric entry on this particle's parent body composition) (Figure 3). The CM mixing line is a conceptual line with 0.7 slope and a δ^{17}O intercept of -4.23‰ originally defined by Clayton and Mayeda (1999) based on the analysis of a small number of CO and CM chondrites (15 and 34, respectively). This line reflects an incomplete mixing process between anhydrous isotopically light solids and an isotopically heavy water component (Clayton & Mayeda, 1999). Although the bulk O-isotope compositions of each carbonaceous chondrite group also define a spread in isotope space consistent with interaction between light solids and heavy water (Ireland et al., 2020), only the CO and CM chondrites are linked by a single line with a shared intercept value. This may imply a closer relationship between these two chondrite groups than their relationship to other groups (i.e., the CO-CM chondrite clan (Weisberg et al., 2006)).

Since the original definition of the CM mixing line, some of the samples analyzed by Clayton and Mayeda (1999) have been reclassified as C2-ung chondrites with affinities to the "CM complex" (e.g., Bells and Essebi; Mittlefehldt, 2002; van Kooten et al., 2020; The Meteoritical Bulletin, 2021, https://www.lpi.usra.edu/meteor/) while a cluster of thermally metamorphosed members with isotopically heavy compositions are now recognized as a distinct chondrite group, the CY chondrites (Ikeda, 1992; King, Bates, et al., 2019). Thus, the CM mixing line appears to link three chondrite groups, the CO, CM, and CY chondrites (Suttle et al., 2020).

The position of the newly discovered ^{16}O-poor micrometeorites on this CM mixing line and occurring at heavier values outside the fields defined known chondrite groups could be evidence for a fourth chondrite group. Together with the CO, CM, and CY chondrites these ^{16}O-poor micrometeorites could be considered a large chondrite clan. This would imply a close link between these four groups, perhaps representing bodies that formed as asteroidal neighbors in a compositionally similar region of the protoplanetary disk as suggested by Schrader and Davidson (2017), with subsequent differences between groups reflecting their local formation environments, and the amount water-ice and other volatiles that they initially accreted (Chaumard et al., 2018; Suttle et al., 2020).

An alternative interpretation would be that these micrometeorites are an extension in O-isotope space of an existing meteorite group. The closest group is the CY chondrites (Figure 3). Recent analysis of additional CM chondrites, such as the new highly primitive Asuka CMs (Kimura et al., 2020) has extended the isotopic range of the CM group to lighter values, meaning that the CO and CM chondrite regions now overlap significantly (as seen in Figure 3). The range currently represented by the CM group spans approximately 18‰ in δ^{18}O. It is conceivable that the CY chondrite range (which, at present is fairly restricted) occupies a similarly large isotopic spread but remains unrealized due to small sample statistics (only 5–9 CY chondrites are known (King, Bates, et al., 2019; Suttle et al., 2021)).
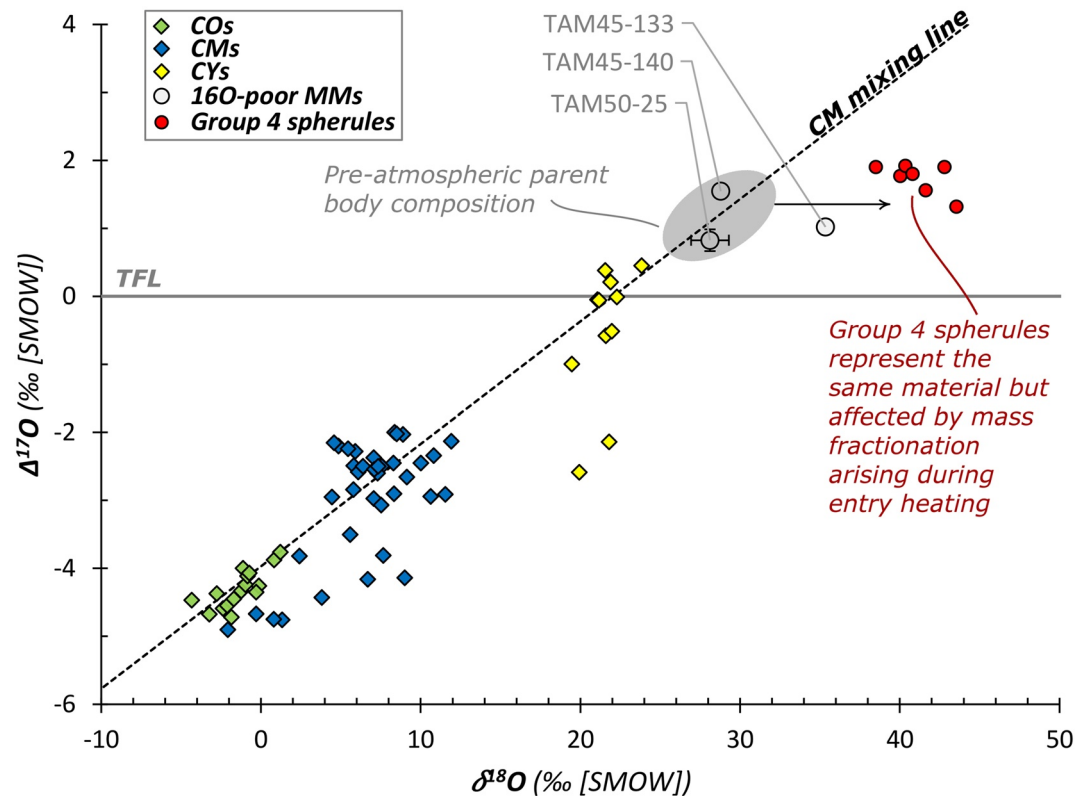
Figure 4. The relationships between the CO, CM, and CY chondrites, the ^{16}O-poor micrometeorites reported in this study and the "group 4" cosmic spherule population. This plot highlights how mass fractionation of the ^{16}O-poor micrometeorite composition (given by TAM45-140 and TAM50-25) will produce the observed values measured for the "group 4" cosmic spherule population (shifted by approximately +10‰ in $\delta^{18}O$ space). This provides a causal link between the two groups, leading to the conclusion that the "group 4" cosmic spherules and the ^{16}O-poor micrometeorites reported here are members of the same population and originate from a hydrated carbonaceous chondrite parent body. Chondrite data taken from Clayton & Mayeda (1999), Moriarty et al. (2009), Ivanova et al. (2010), Lee et al. (2016, 2019), Bouvier, Gattacceca, Agee, et al. (2017), Bouvier, Gattacceca, Grossman, et al. (2017), King, Russell, et al. (2019), Gattacceca et al. (2019), and Kimura et al. (2020). "Group 4" compositions (shown in Table 2) were taken from Yada et al. (2005), Suavet et al. (2010), and Goderis et al. (2020). Note, analytical uncertainties ($\delta^{18}O$: ±0.4‰, $\Delta^{17}O$: ±0.024‰) for the two ^{16}O-poor micrometeorites (TAM45-133 and TAM45-140) are smaller than the symbols.

Whether the micrometeorites analyzed here are samples of a new chondrite group or members of the CY chondrites is not clear. All known CY chondrites share a similar alteration history; aqueous alteration followed by pronounced thermal metamorphism (Ikeda, 1992; King, Bates, et al., 2019; Suttle et al., 2021) with peak temperatures >500°C (Nakamura, 2005). Their matrices lack hydrated phyllosilicates (King, Bates, et al., 2019). By contrast, the presence of igneous rims observed on all three of the ^{16}O-poor micrometeorites is evidence that they initially had hydrated phyllosilicate prior to atmospheric entry (Genge, 2006; Genge et al., 2017). Thus, these micrometeorites are either CY chondrites which avoided the post-hydration parent body heating characteristic of all known CYs or they are members of a different chondrite group which did not experience metamorphic heating. Unfortunately, with the current evidence and relatively small number of samples these two scenarios cannot be distinguished.

2. The position of these ^{16}O-poor micrometeorites is interesting for an additional reason. Several previous bulk O-isotope studies on micrometeorites (primarily melted cosmic spherules) have reported particles with unusual and closely related ^{16}O-poor compositions (Table 3, Figure 4). Members of this group were originally reported by Yada et al. (2005) and later explicitly defined by Suavet et al. (2010) who termed this population "group 4," because their sample of micrometeorites neatly split into four distinct regions in O-isotope space (with the remaining three groups confidently linked back to know chondrite groups). Subsequent independent research has continued to report additional "group 4" spherules (e.g., Goderis et al., 2020), but their parent
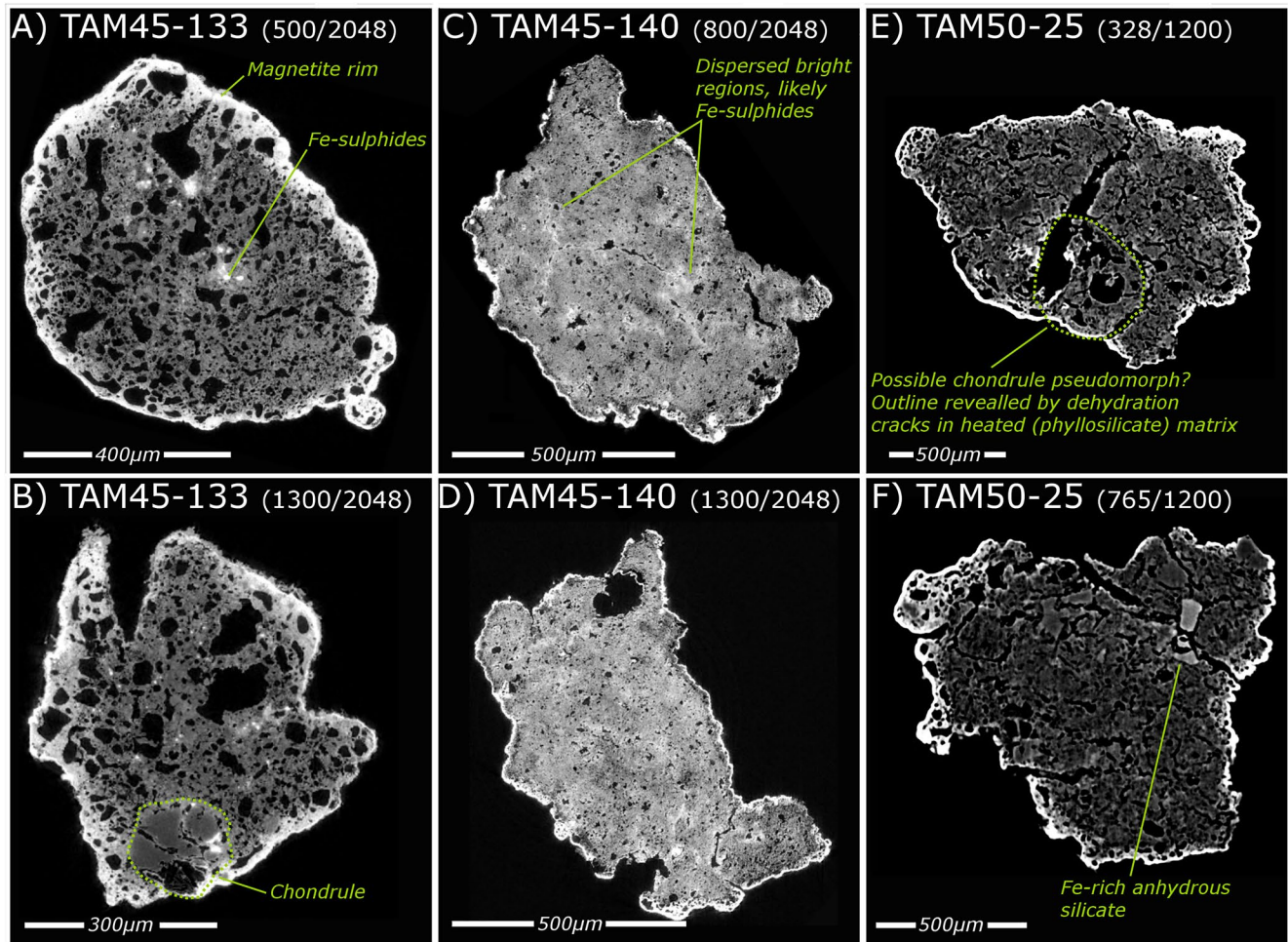
Figure 5. Micro-CT images showing additional slices through the three ^{16}O-poor micrometeorites (a and b: TAM45-133, c and d: TAM45-140, and e and f: TAM50-25) allowing more of their unmelted parent body texture to be studied. Anhydrous silicates are rare (observed in panels (b and f)) matrix cation chemistry (Mg/Fe ratios) is variable across particles. Fe-sulfides are identifiable in most particles.

body affinities have remained unidentified. This is largely because identifying micrometeorites with anomalous O-isotope compositions without also destroying the target particles during the measurement process is difficult (owing to the small sample masses involved). Additionally, studying cosmic spherules, which experienced complete melting during entry means that parent body textures are not preserved.

To resolve this situation Suttle et al. (2020) focused on unmelted and scoriaceous particles and paired μCT pre-characterization with O-isotope mass spectrometry. They found a single particle (TAM50-25) whose O-isotope composition was consistent with the expected value for a group 4 particle prior to atmospheric entry induced mass fractionation. We repeated the methodology of Suttle et al. (2020) and identified an additional two particles (TAM45-140 and TAM45-133). These three micrometeorites are probably precursors of the "group 4" cosmic spherules, providing examples of this population's texture and parentage. We therefore conclude that the "group 4" spherules are samples of a hydrated carbonaceous chondrite.

Combining the results of Suttle et al. (2020) and this study allows a very approximate estimate of the abundance of ^{16}O-poor materials among the coarsest size fractions (>400 μm) of the micrometeorite flux. This gives a value of ~14% ($N = 21$). Despite low sample statistics our value is close to the abundance of ^{16}O-poor materials calculated by Cordier and Folco (2014) who arrived at values of 6%–17% based on the analysis of fully melted cosmic spherules.

Table 3
Cosmic Spherules Whose Bulk O-Isotope Compositions Define the Enigmatic ¹⁶O-Poor "Group 4" Population (Shown in Black)

Particle ID	Diameter (μm)	Subtype	$\delta^{17}O$	$\delta^{18}O$	$\Delta^{17}O$	Collection	References
WF1202B-0065	586	BO	22.59	40.03	1.77	WF	Goderis et al. (2020)
WF1202B-0062	600	CC	22.9	40.34	1.92	WF	Goderis et al. (2020)
WF1202B-0070	450	PO	23.2	41.62	1.56	WF	Goderis et al. (2020)
WF1202B-0059	656	V	23.96	43.54	1.32	WF	Goderis et al. (2020)
D2	>500	V	23	40.8	1.8	TAM	Suavet et al. (2010) EPSL
D1	>500	V	24.2	42.8	1.9	TAM	Suavet et al. (2010) EPSL
KW54087	50–300	BO	22	38.5	1.9	Dome Fuji	Yada et al. (2005) GCA
KW540299	50–300	Glass	29.4	48.5	4.2	Dome Fuji	Yada et al. (2005) GCA
WF1202B-0220	210–350	V	21.8	39.5	1.3	WF	Lampe et al. (2022)
M03KS063 AVG	50–300	CC	40	51.8	13	Dome Fuji	Yada et al. (2005) GCA
M03KS021	50–300	CC	34	56.5	4.6	Dome Fuji	Yada et al. (2005) GCA
KW540100 AVG	50–300	CC	15.3	25.2	2.2	Dome Fuji	Yada et al. (2005) GCA
10.11	670	CC	31.4	17.20	0.80	Atacama	Van Ginneken et al. (2017)
10.13	700	CC	42.6	23.50	1.40	Atacama	Van Ginneken et al. (2017)
WF1202B-0207	210–350	V	34.8	64.2	1.4	WF	Lampe et al. (2022)

Note. Also given are other particles with anomalous ¹⁶O-poor compositions that span a huge range in O-isotope space (shown in gray).

5. Conclusions

This study used the combination of textural characterization through non-destructive tomography and subsequent O-isotope analysis to evaluate the probable parentage of large (420–820 μm) micrometeorites. Studying the coarse size fractions of the cosmic dust flux bridges the knowledge gap between insights from smaller micrometeorites and larger (cm-scale) meteorites. It also expands our knowledge of the geological diversity of the solar system through the discovery of new and otherwise unsampled planetary materials.

This investigation identified two ¹⁶O-poor particles. Their textures and inferred mineralogy demonstrate a clear link to the hydrated carbonaceous chondrites. Furthermore, their position in O-isotope space suggests that they are either an extension of the CY group or a new and unrecognized chondrite group. Further dedicated study is required to resolve the possibilities. We recommend the non-destructive identification of new micrometeorites originating from the ¹⁶O-poor group followed by detailed evaluation of their chemistry, texture and alteration histories. Finally, the ¹⁶O-poor micrometeorites described in this study are interpreted as unmelted members of the anomalous "group 4" cosmic spherule population (now widely reported in the literature), preserving a composition less-affected by atmospheric entry mass fractionation. If correct, this discovery reveals that the group "4 spherules" come from a hydrated C-type asteroid source.

Data Availability Statement

The authors confirm that all the data supporting the findings of this study are mostly available within the article itself. In addition, all data used in this work is available as a direct download from https://doi.org/10.17632/8yrn4bfhv8.1.

References

Baecker, B., Ott, U., Cordier, C., Folco, L., Trieloff, M., van Ginneken, M., & Rochette, P. (2018). Noble gases in micrometeorites from the Transantarctic Mountains. *Geochimica et Cosmochimica Acta*, *242*, 266–297. https://doi.org/10.1016/j.gca.2018.08.027

Battandier, M., Bonal, L., Quirico, E., Beck, P., Engrand, C., Duprat, J., & Dartois, E. (2018). Characterization of the organic matter and hydration state of Antarctic micrometeorites: A reservoir distinct from carbonaceous chondrites. *Icarus*, *306*, 74–93. https://doi.org/10.1016/j.icarus.2018.02.002

Bischoff, A., Vogel, N., & Roszjar, J. (2011). The Rumuruti chondrite group. *Geochemistry*, *71*(2), 101–133. https://doi.org/10.1016/j.chemer.2011.02.005

Bouvier, A., Gattacceca, J., Agee, C., Grossman, J., & Metzler, K. (2017). The Meteoritical Bulletin, No. 104. *Meteoritics & Planetary Sciences*, *52*(10), 2284. https://doi.org/10.1111/maps.12930

Bouvier, A., Gattacceca, J., Grossman, J., & Metzler, K. (2017). The Meteoritical Bulletin, No. 105. *Meteoritics & Planetary Sciences*, *52*, 2411.

Burns, J. A., Lamy, P. L., & Soter, S. (1979). Radiation forces on small particles in the solar system. *Icarus*, *40*, 1–48. https://doi.org/10.1016/0019-1035(79)90050-2

Chaumard, N., Defouilloy, C., & Kita, N. T. (2018). Oxygen isotope systematics of chondrules in the Murchison CM2 chondrite and implications for the CO-CM relationship. *Geochimica et Cosmochimica Acta*, *228*, 220–242. https://doi.org/10.1016/j.gca.2018.02.040

Clayton, R. N., & Mayeda, T. K. (1996). Oxygen isotope studies of achondrites. *Geochimica et Cosmochimica Acta*, *60*(11), 1999–2017. https://doi.org/10.1016/0016-7037(96)00074-9

Clayton, R. N., & Mayeda, T. K. (1999). Oxygen isotope studies of carbonaceous chondrites. *Geochimica et Cosmochimica Acta*, *63*(13–14), 2089–2104. https://doi.org/10.1016/s0016-7037(99)00090-3

Clayton, R. N., Mayeda, T. K., Goswami, J. N., & Olsen, E. J. (1991). Oxygen isotope studies of ordinary chondrites. *Geochimica et Cosmochimica Acta*, *55*(8), 2317–2337. https://doi.org/10.1016/0016-7037(91)90107-g

Clayton, R. N., Mayeda, T. K., & Rubin, A. E. (1984). Oxygen isotopic compositions of enstatite chondrites and aubrites. *Journal of Geophysical Research*, *89*(S01), C245–C249. https://doi.org/10.1029/jb089is01p0c245

Cordier, C., Baecker, B., Ott, U., Folco, L., & Trieloff, M. (2018). A new type of oxidized and pre-irradiated micrometeorite. *Geochimica et Cosmochimica Acta*, *233*, 135–158. https://doi.org/10.1016/j.gca.2018.04.010

Cordier, C., & Folco, L. (2014). Oxygen isotopes in cosmic spherules and the composition of the near Earth interplanetary dust complex. *Geochimica et Cosmochimica Acta*, *146*, 18–26. https://doi.org/10.1016/j.gca.2014.09.038

Cordier, C., Folco, L., Suavet, C., Sonzogni, C., & Rochette, P. (2011). Major, trace element and oxygen isotope study of glass cosmic spherules of chondritic composition: The record of their source material and atmospheric entry heating. *Geochimica et Cosmochimica Acta*, *75*(18), 5203–5218. https://doi.org/10.1016/j.gca.2011.06.014

Dionnet, Z., Suttle, M. D., Longobardo, A., Rotundi, A., Folco, L., Della Corte, V., & King, A. (2020). X-ray computed tomography: Morphological and porosity characterization of giant Antarctic micrometeorites. *Meteoritics & Planetary Sciences*, *55*(7), 1581–1599. https://doi.org/10.1111/maps.13533

Dobrică, E., Ogliore, R. C., Engrand, C., Nagashima, K., & Brearley, A. J. (2019). Mineralogy and oxygen isotope systematics of magnetite grains and a magnetite-dolomite assemblage in hydrated fine-grained Antarctic micrometeorites. *Meteoritics & Planetary Sciences*, *54*(9), 1973–1989. https://doi.org/10.1111/maps.13366

Engrand, C., & Maurette, M. (1998). Carbonaceous micrometeorites from Antarctica. *Meteoritics & Planetary Science*, *33*(4), 565–580. https://doi.org/10.1111/j.1945-5100.1998.tb01665.x

Folco, L., & Cordier, C. (2015). Micrometeorites. *EMU Notes in Mineralogy*, *15*, 253–297.

Gattacceca, J., Bouvier, A., Grossman, J., Metzler, K., & Uehara, M. (2019). The Meteoritical Bulletin, No. 106. *Meteoritics & Planetary Science*, *54*(2), 469–471. https://doi.org/10.1111/maps.13215

Genge, M. J. (2006). Igneous rims on micrometeorites. *Geochimica et Cosmochimica Acta*, *70*(10), 2603–2621. https://doi.org/10.1016/j.gca.2006.02.005

Genge, M. J. (2017). Vesicle dynamics during the atmospheric entry heating of cosmic spherules. *Meteoritics & Planetary Sciences*, *52*(3), 443–457. https://doi.org/10.1111/maps.12805

Genge, M. J., Engrand, C., Gounelle, M., & Taylor, S. (2008). The classification of micrometeorites. *Meteoritics & Planetary Sciences*, *43*(3), 497–515. https://doi.org/10.1111/j.1945-5100.2008.tb00668.x

Genge, M. J., Gileski, A., & Grady, M. M. (2005). Chondrules in Antarctic micrometeorites. *Meteoritics & Planetary Sciences*, *40*(2), 225–238. https://doi.org/10.1111/j.1945-5100.2005.tb00377.x

Genge, M. J., Suttle, M., & Van Ginneken, M. (2016). Olivine settling in cosmic spherules during atmospheric deceleration: An indicator of the orbital eccentricity of interplanetary dust. *Geophysical Research Letters*, *43*(20), 10–646. https://doi.org/10.1002/2016gl070874

Genge, M. J., Suttle, M., & Van Ginneken, M. (2017). Thermal shock fragmentation of Mg silicates within scoriaceous micrometeorites reveal hydrated asteroidal sources. *Geology*, *45*(10), 891–894. https://doi.org/10.1130/g39426.1

Goderis, S., Soens, B., Huber, M. S., McKibbin, S., Van Ginneken, M., Van Maldeghem, F., et al. (2020). Cosmic spherules from Widerøefjellet, Sør Rondane Mountains (East Antarctica). *Geochimica et Cosmochimica Acta*, *270*, 112–143. https://doi.org/10.1016/j.gca.2019.11.016

Greenwood, R. C., Franchi, I. A., Gibson, J. M., & Benedix, G. K. (2012). Oxygen isotope variation in primitive achondrites: The influence of primordial, asteroidal and terrestrial processes. *Geochimica et Cosmochimica Acta*, *94*, 146–163. https://doi.org/10.1016/j.gca.2012.06.025

Greshake, A., Kloeck, W., Arndt, P., Maetz, M., Flynn, G. J., Bajt, S., & Bischoff, A. (1998). Heating experiments simulating atmospheric entry heating of micrometeorites: Clues to their parent body sources. *Meteoritics & Planetary Science*, *33*(2), 267–290. https://doi.org/10.1111/j.1945-5100.1998.tb01632.x

Heck, P. R., Schmitz, B., Rout, S. S., Tenner, T., Villalon, K., Cronholm, A., et al. (2016). A search for H-chondritic chromite grains in sediments that formed immediately after the breakup of the L-chondrite parent body 470 Ma ago. *Geochimica et Cosmochimica Acta*, *177*, 120–129. https://doi.org/10.1016/j.gca.2015.11.042

Ikeda, Y. (1992). An overview of the research consortium, "Antarctic carbonaceous chondrites with CI affinities, Yamato-86720, Yamato-82162, and Belgica-7904". *Antarctic Meteorite Research*, *5*, 49–73.

Ireland, T. R., Avila, J., Greenwood, R. C., Hicks, L. J., & Bridges, J. C. (2020). Oxygen isotopes and sampling of the solar system. *Space Science Reviews*, *216*(2), 1–60. https://doi.org/10.1007/s11214-020-0645-3

Ivanova, M. A., Lorenz, C. A., Nazarov, M. A., Brandstaetter, F., Franchi, I. A., Moroz, L. V., et al. (2010). Dhofar 225 and Dhofar 735: Relationship to CM2 chondrites and metamorphosed carbonaceous chondrites, Belgica-7904 and Yamato-86720. *Meteoritics & Planetary Science*, *45*(7), 1108–1123. https://doi.org/10.1111/j.1945-5100.2010.01064.x

Ketcham, R. A., & Carlson, W. D. (2001). Acquisition, optimization and interpretation of X-ray computed tomographic imagery: Applications to the geosciences. *Computational Geosciences*, *27*(4), 381–400. https://doi.org/10.1016/s0098-3004(00)00116-3

Kimura, M., Imae, N., Komatsu, M., Barrat, J. A., Greenwood, R. C., Yamaguchi, A., & Noguchi, T. (2020). The most primitive CM chondrites, Asuka 12085, 12169, and 12236, of subtypes 3.0–2.8: Their characteristic features and classification. *Policy Sciences*, *26*, 100565. https://doi.org/10.1016/j.polar.2020.100565

King, A. J., Bates, H. C., Krietsch, D., Busemann, H., Clay, P. L., Schofield, P. F., & Russell, S. S. (2019). The Yamato-type (CY) carbonaceous chondrite group: Analogues for the surface of asteroid Ryugu? *Geochemistry*, *79*(4), 125531. https://doi.org/10.1016/j.chemer.2019.08.003

King, A. J., Russell, S. S., Schofield, P. F., Humphreys-Williams, E. R., Strekopytov, S., Abernethy, F. A. J., et al. (2019). The alteration history of the Jbilet Winselwan CM carbonaceous chondrite: An analog for C-type asteroid sample return. *Meteoritics & Planetary Science*, *54*, 521–543.

King, A. J., Solomon, J. R., Schofield, P. F., & Russell, S. S. (2015). Characterising the CI and CI-like carbonaceous chondrites using thermogravimetric analysis and infrared spectroscopy. *Earth Planets and Space*, *67*, 1–12. https://doi.org/10.1186/s40623-015-0370-4

Krot, A. N., & Rubin, A. E. (1996). Microchondrule-bearing chondrule rims: Constraints on chondrule formation, Chapter 9. In R. H. Hewins, R. H. Jones, & E. R. D. Scott (Eds.), *Chondrules and the protoplanetary disk* (pp. 181–184). Cambridge University Press.

Kurat, G., Koeberl, C., Presper, T., Brandstätter, F., & Maurette, M. (1994). Petrology and geochemistry of Antarctic micrometeorites. *Geochimica et Cosmochimica Acta*, *58*(18), 3879–3904. https://doi.org/10.1016/0016-7037(94)90369-7

Lampe, S., Soens, B., Chernonozhkin, S. M., de Vega, C. G., Van Ginneken, M., Van Maldeghem, F., et al. (2022). Decoupling of chemical and isotope fractionation processes during atmospheric heating of micrometeorites. *Geochimica et Cosmochimica Acta*, *324*, 221–239. https://doi.org/10.1016/j.gca.2022.02.008

Lee, M. R., Cohen, B. E., King, A. J., & Greenwood, R. C. (2019). The diversity of CM carbonaceous chondrite parent bodies explored using Lewis Cliff 85311. *Geochimica et Cosmochimica Acta*, *264*, 224–244. https://doi.org/10.1016/j.gca.2019.07.027

Lee, M. R., Lindgren, P., King, A. J., Greenwood, R. C., Franchi, I. A., & Sparkes, R. (2016). Elephant Moraine 96029, a very mildly aqueously altered and heated CM carbonaceous chondrite: Implications for the drivers of parent body processing. *Geochimica et Cosmochimica Acta*, *187*, 237–259. https://doi.org/10.1016/j.gca.2016.05.008

Lindgren, P., Hanna, R. D., Dobson, K. J., Tomkinson, T., & Lee, M. R. (2015). The paradox between low shock-stage and evidence for compaction in CM carbonaceous chondrites explained by multiple low-intensity impacts. *Geochimica et Cosmochimica Acta*, *148*, 159–178. https://doi.org/10.1016/j.gca.2014.09.014

Love, S. G., & Brownlee, D. E. (1993). A direct measurement of the terrestrial mass accretion rate of cosmic dust. *Science*, *262*(5133), 550–553. https://doi.org/10.1126/science.262.5133.550

Matrajt, G., Messenger, S., Brownlee, D., & Joswiak, D. (2012). Diverse forms of primordial organic matter identified in interplanetary dust particles. *Meteoritics & Planetary Science*, *47*(4), 525–549. https://doi.org/10.1111/j.1945-5100.2011.01310.x

Mirone, A., Brun, E., Gouillart, E., Tafforeau, P., & Kieffer, J. (2014). The PyHST2 hybrid distributed code for high-speed tomographic reconstruction with iterative reconstruction and a priori knowledge capabilities. *Nuclear Instruments and Methods in Physics Research B*, *324*, 41–48. https://doi.org/10.1016/j.nimb.2013.09.030

Mittlefehldt, D. W. (2002). Geochemistry of the ungrouped carbonaceous chondrite Tagish Lake, the anomalous CM chondrite Bells, and comparison with CI and CM chondrites. *Meteoritics & Planetary Science*, *37*(5), 703–712. https://doi.org/10.1111/j.1945-5100.2002.tb00850.x

Moriarty, G. M., Rumble, D., III, & Friedrich, J. M. (2009). Compositions of four unusual CM or CM-related Antarctic chondrites. *Geochemistry*, *69*(2), 161–168. https://doi.org/10.1016/j.chemer.2008.12.002

Nakamura, T. (2005). Post-hydration thermal metamorphism of carbonaceous chondrites. *Journal of Mineralogical and Petrological Sciences*, *100*(6), 260–272. https://doi.org/10.2465/jmps.100.260

Noguchi, T., Ohashi, N., Tsujimoto, S., Mitsunari, T., Bradley, J. P., Nakamura, T., et al. (2015). Cometary dust in Antarctic ice and snow: Past and present chondritic porous micrometeorites preserved on the Earth's surface. *Earth and Planetary Science Letters*, *410*, 1–11. https://doi.org/10.1016/j.epsl.2014.11.012

Pack, A. (2021). Isotopic traces of atmospheric O_2 in rocks, minerals, and melts. *Reviews in Mineralogy and Geochemistry*, *86*(1), 217–240. https://doi.org/10.2138/rmg.2021.86.07

Pack, A., Höweling, A., Hezel, D. C., Stefanak, M., Beck, A. K., Peters, S. T. M., et al. (2017). Tracing the oxygen isotope composition of the upper Earth atmosphere using cosmic spherules. *Nature Communications*, *8*(1), 15702. https://doi.org/10.1038/ncomms15702

Pack, A., Tanaka, R., Hering, M., Sengupta, S., Peters, S., & Nakamura, E. (2016). The oxygen isotope composition of San Carlos olivine on the VSMOW2-SLAP2 scale. *Rapid Communications in Mass Spectrometry*, *30*(13), 1495–1504. https://doi.org/10.1002/rcm.7582

Rochette, P., Folco, L., Suavet, C., van Ginneken, M., Gattacceca, J., Perchiazzi, N., et al. (2008). Micrometeorites from the Transantarctic Mountains. *Proceedings of the National Academy of Sciences*, *105*(47), 18206–18211. https://doi.org/10.1073/pnas.0806049105

Rudraswami, N. G., Genge, M. J., Marrocchi, Y., Villeneuve, J., & Taylor, S. (2020). The oxygen isotope compositions of large numbers of small cosmic spherules: Implications for their sources and the isotopic composition of the upper atmosphere. *Journal of Geophysical Research: Planets*, *125*(10), e2020JE006414. https://doi.org/10.1029/2020je006414

Rudraswami, N. G., Marrocchi, Y., Shyam Prasad, M., Fernandes, D., Villeneuve, J., & Taylor, S. (2019). Oxygen isotopic and chemical composition of chromites in micrometeorites: Evidence of ordinary chondrite precursors. *Meteoritics & Planetary Science*, *54*(6), 1347–1361. https://doi.org/10.1111/maps.13281

Rudraswami, N. G., Suttle, M. D., Marrocchi, Y., Taylor, S., & Villeneuve, J. (2022). In-situ O-isotope analysis of relict spinel and forsterite in small (<200 μm) Antarctic micrometeorites–Samples of chondrules & CAIs from carbonaceous chondrites. *Geochimica et Cosmochimica Acta*, *325*, 1–24. https://doi.org/10.1016/j.gca.2022.03.015

Schrader, D. L., & Davidson, J. (2017). CM and CO chondrites: A common parent body or asteroidal neighbors? Insights from chondrule silicates. *Geochimica et Cosmochimica Acta*, *214*, 157–171. https://doi.org/10.1016/j.gca.2017.07.031

Schrader, D. L., Franchi, I. A., Connolly, H. C., Jr., Greenwood, R. C., Lauretta, D. S., & Gibson, J. M. (2011). The formation and alteration of the Renazzo-like carbonaceous chondrites I: Implications of bulk-oxygen isotopic composition. *Geochimica et Cosmochimica Acta*, *75*(1), 308–325. https://doi.org/10.1016/j.gca.2010.09.028

Schrader, D. L., Nagashima, K., Krot, A. N., Ogliore, R. C., & Hellebrand, E. (2014). Variations in the O-isotope composition of gas during the formation of chondrules from the CR chondrites. *Geochimica et Cosmochimica Acta*, *132*, 50–74. https://doi.org/10.1016/j.gca.2014.01.034

Sharp, Z. D. (1990). A laser-based microanalytical method for the in situ determination of oxygen isotope ratios of silicates and oxides. *Geochimica et Cosmochimica Acta*, *54*(5), 1353–1357. https://doi.org/10.1016/0016-7037(90)90160-m

Sharp, Z. D., Gibbons, J. A., Maltsev, O., Atudorei, V., Pack, A., Sengupta, S., et al. (2016). A calibration of the triple oxygen isotope fractionation in the SiO_2-H_2O system and applications to natural samples. *Geochimica et Cosmochimica Acta*, *186*, 105–119. https://doi.org/10.1016/j.gca.2016.04.047

Shearer, C. K., Burger, P., & Papike, J. J. (2010). Petrogenetic relationships between diogenites and olivine diogenites: Implications for magmatism on the HED parent body. *Geochimica et Cosmochimica Acta*, *74*(16), 4865–4880. https://doi.org/10.1016/j.gca.2010.05.015

Suavet, C., Alexandre, A., Franchi, I. A., Gattacceca, J., Sonzogni, C., Greenwood, R. C., et al. (2010). Identification of the parent bodies of micrometeorites with high-precision oxygen isotope ratios. *Earth and Planetary Science Letters*, *293*(3–4), 313–320. https://doi.org/10.1016/j.epsl.2010.02.046

Suttle, M. D., Dionnet, Z., Franchi, I., Folco, L., Gibson, J., Greenwood, R. C., et al. (2020). Isotopic and textural analysis of giant unmelted micrometeorites–identification of new material from intensely altered ^{16}O-poor water-rich asteroids. *Earth and Planetary Science Letters*, *546*, 116444. https://doi.org/10.1016/j.epsl.2020.116444

Suttle, M. D., & Folco, L. (2020). The extraterrestrial dust flux: Size distribution and mass contribution estimates inferred from the Transantarctic Mountains (TAM) micrometeorite collection. *Journal of Geophysical Research: Planets*, *125*(2), e2019JE006241. https://doi.org/10.1029/2019je006241

Suttle, M. D., Genge, M. J., Folco, L., & Russell, S. S. (2017). The thermal decomposition of fine-grained micrometeorites, observations from mid-IR spectroscopy. *Geochimica et Cosmochimica Acta*, *206*, 112–136. https://doi.org/10.1016/j.gca.2017.03.002

Suttle, M. D., Genge, M. J., Folco, L., Van Ginneken, M., Lin, Q., Russell, S. S., & Najorka, J. (2019). The atmospheric entry of fine-grained micrometeorites: The role of volatile gases in heating and fragmentation. *Meteoritics & Planetary Science*, *54*(3), 503–520. https://doi.org/10.1111/maps.13220

Suttle, M. D., Genge, M. J., & Russell, S. S. (2017). Shock fabrics in fine-grained micrometeorites. *Meteoritics & Planetary Science*, *52*(10), 2258–2274. https://doi.org/10.1111/maps.12927

Suttle, M. D., Greshake, A., King, A. J., Schofield, P. F., Tomkins, A., & Russell, S. S. (2021). The alteration history of the CY chondrites, investigated through analysis of a new member: Dhofar 1988. *Geochimica et Cosmochimica Acta*, *295*, 286–309. https://doi.org/10.1016/j.gca.2020.11.008

Taylor, S., Jones, K. W., Herzog, G. F., & Hornig, C. E. (2011). Tomography: A window on the role of sulfur in the structure of micrometeorites. *Meteoritics & Planetary Science*, *46*(10), 1498–1509. https://doi.org/10.1111/j.1945-5100.2011.01245.x

Taylor, S., Lever, J. H., & Harvey, R. P. (1998). Accretion rate of cosmic spherules measured at the South Pole. *Nature*, *392*(6679), 899–903. https://doi.org/10.1038/31894

Taylor, S., Matrajt, G., & Guan, Y. (2012). Fine-grained precursors dominate the micrometeorite flux. *Meteoritics & Planetary Science*, *47*(4), 550–564. https://doi.org/10.1111/j.1945-5100.2011.01292.x

Thiemens, M. H., Jackson, T., Zipf, E. C., Erdman, P. W., & van Egmond, C. (1995). Carbon dioxide and oxygen isotope anomalies in the mesosphere and stratosphere. *Science*, *270*(5238), 969–972. https://doi.org/10.1126/science.270.5238.969

Toppani, A., Libourel, G., Engrand, C., & Maurette, M. (2001). Experimental simulation of atmospheric entry of micrometeorites. *Meteoritics & Planetary Science*, *36*(10), 1377–1396. https://doi.org/10.1111/j.1945-5100.2001.tb01831.x

Van Ginneken, M., Folco, L., Cordier, C., & Rochette, P. (2012). Chondritic micrometeorites from the Transantarctic Mountains. *Meteoritics & Planetary Science*, *47*(2), 228–247. https://doi.org/10.1111/j.1945-5100.2011.01322.x

Van Ginneken, M., Gattacceca, J., Rochette, P., Sonzogni, C., Alexandre, A., Vidal, V., & Genge, M. J. (2017). The parent body controls on cosmic spherule texture: Evidence from the oxygen isotopic compositions of large micrometeorites. *Geochimica et Cosmochimica Acta*, *212*, 196–210. https://doi.org/10.1016/j.gca.2017.05.008

Van Ginneken, M., Genge, M. J., Folco, L., & Harvey, R. P. (2016). The weathering of micrometeorites from the Transantarctic Mountains. *Geochimica et Cosmochimica Acta*, *179*, 1–31. https://doi.org/10.1016/j.gca.2015.11.045

van Kooten, E., Cavalcante, L., Wielandt, D., & Bizzarro, M. (2020). The role of Bells in the continuous accretion between the CM and CR chondrite reservoirs. *Meteoritics & Planetary Science*, *55*(3), 575–590. https://doi.org/10.1111/maps.13459

Weisberg, M. K., & Kimura, M. (2012). The unequilibrated enstatite chondrites. *Geochemistry*, *72*(2), 101–115. https://doi.org/10.1016/j.chemer.2012.04.003

Weisberg, M. K., McCoy, T. J., & Krot, A. N. (2006). Systematics and evaluation of meteorite classification. *Meteorites and the Early Solar System II*, *19*, 19–52.

Weisberg, M. K., Prinz, M., Clayton, R. N., Mayeda, T. K., Grady, M. M., Franchi, I., et al. (1996). The K (Kakangari) chondrite grouplet. *Geochimica et Cosmochimica Acta*, *60*(21), 4253–4263. https://doi.org/10.1016/s0016-7037(96)00233-5

Wlotzka, F. (2005). Cr spinel and chromite as petrogenetic indicators in ordinary chondrites: Equilibration temperatures of petrologic types 3.7 to 6. *Meteoritics & Planetary Science*, *40*(11), 1673–1702. https://doi.org/10.1111/j.1945-5100.2005.tb00138.x

Wostbrock, J. A. G., Cano, E. J., & Sharp, Z. D. (2020). An internally consistent triple oxygen isotope calibration of standards for silicates, carbonates and air relative to VSMOW2 and SLAP2. *Chemical Geology*, *533*, 11932. https://doi.org/10.1016/j.chemgeo.2019.119432

Yada, T., Nakamura, T., Noguchi, T., Matsumoto, N., Kusakabe, M., Hiyagon, H., et al. (2005). Oxygen isotopic and chemical compositions of cosmic spherules collected from the Antarctic ice sheet: Implications for their precursor materials. *Geochimica et Cosmochimica Acta*, *69*(24), 5789–5804. https://doi.org/10.1016/j.gca.2005.08.002

Young, E. D., & Russell, S. S. (1998). Oxygen reservoirs in the early solar nebula inferred from an Allende CAI. *Science*, *282*(5388), 452–455. https://doi.org/10.1126/science.282.5388.452

Yurimoto, H., Krot, A. N., Choi, B. G., Aléon, J., Kunihiro, T., & Brearley, A. J. (2008). Oxygen isotopes of chondritic components. *Reviews in Mineralogy and Geochemistry*, *68*(1), 141–186. https://doi.org/10.2138/rmg.2008.68.8